

ON THE DEVELOPMENT OF A DESIGN FRAMEWORK FOR AEROELASTICALLY SCALED WING MODELS BASED ON TOPOLOGY OPTIMISATION WITH ADDITIVE MANUFACTURING CONSTRAINTS

Vasco Coelho^{1,2}, Bernardo Leite^{3,2}, Frederico Afonso², Alain de Souza², Fernando Lau²,
Afzal Suleman^{2,3}

¹Portuguese Air Force Academy
Granja do Marquês, 2715-311 Pêro Pinheiro, Portugal
vlcoelho@academiafa.edu.pt

²IDMEC, Instituto Superior Técnico, Universidade de Lisboa
Av. Rovisco Pais, 1049-100 Lisbon, Portugal
frederico.afonso@tecnico.ulisboa.pt
alain.souza@tecnico.ulisboa.pt
lau@tecnico.ulisboa.pt

³Department of Mechanical Engineering, University of Victoria
PO Box 1700, Stn. CSCregain, British Columbia, V8W 2Y2, Canada
bcleite@uvic.ca
suleman@uvic.ca

Keywords: Aeroelastic Scaling, Non-linear Analysis, Topology Optimisation, X-56A

Abstract: The objective of this paper is to present an aeroelastic scaling framework that can be used to create 3D printable prototypes for wind tunnel testing. This would enable the study of aeroelastic phenomena, including nonlinear effects such as the impact of large deformations on classical bending-torsion flutter at a reduced development cost. To this end, an investigation of various scaling laws based on topology optimisation techniques and additive manufacturing constraints to produce scaled wind tunnel models is presented. Additionally, aeroelastic scaling strategies combining aerodynamic similitude by maintaining the outer mould line of the full-size model while tailoring the internal structure using a mix of topology optimisation and sizing are presented. The internal structure can be tailored to integrate sensors and actuators, while the topology optimisation can achieve dynamic similitude. The subject of the case study is the X-56 aircraft.

1 INTRODUCTION

A. Current trends in commercial aviation

With the current pursuit for greener and more efficient air travel, the aviation industry is trying to increase the design space on all the areas within aircraft design, whether on investing in more efficient engines, less carbon-intensive fuels, better structural and aerodynamic properties or new and emerging configurations [1].

Looking at the actual fleet of commercial jet aircraft design, the tendency to increase the aspect ratio (AR) of the wings is evident [2], as shown in Figure 1. Higher AR wings have better

aerodynamic properties as they produce smaller wingtip vortices, thus decreasing induced drag. An overall reduction in drag decreases the fuel consumption, allowing longer and more efficient flights [3]. Nevertheless, these wings tend to be heavier as they are subjected to higher stresses, mainly at the wing root. Additionally, the flexibility of the wing is also increased, which leads to higher deflections, affecting the dynamic behaviour of the airplane. This effect will have an impact on the aircraft aeroelastic properties which might affect its flight envelope [4].

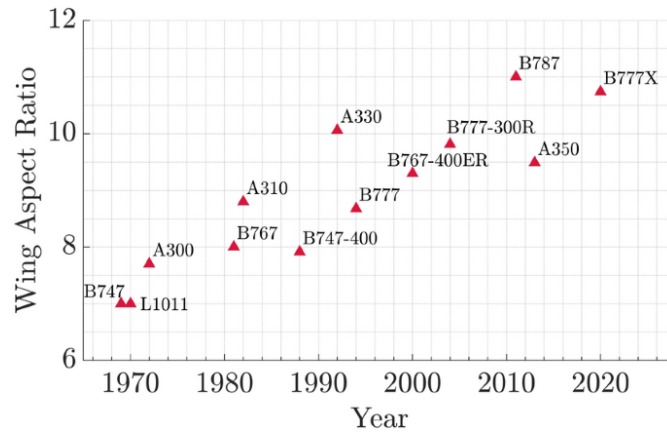


Figure 1: Aspect ratio of commercial jets vs year of entry into service. Retrieved from [2].

B. Aeroelasticity and Scaling

With wings becoming longer and more flexible, being able to predict their dynamic behaviour under all flight regimes becomes a must. Accurately predicting the aeroelastic effects is difficult due to non-linear deflections and requires a coupled high-fidelity fluid-structure solver using Computational Fluid Dynamics (CFD) and Finite Elements Methods (FEM). These analyses are extremely time-consuming and are usually done at a later stage of the design and certification phase of a project. At earlier stages of the design phase, having low-fidelity tools available to estimate the aircraft's aeroelasticity properties becomes relevant [5].

While aeroelastic computational tools might predict the dynamic behaviour of the aircraft, during the design phase, these are usually followed by experimental analysis and testing, including Static Loads Testing, Ground Vibration Testing (GVT) and Wind-tunnel Testing. To carry out this phase of testing campaign, test facilities restrictions, such as dimensions of the wind tunnel or its maximum flow speed may prevent the testing of full scale aircraft model [6]. In this context, the development of aeroelastic scaled models has emerged as an expeditious and cost-friendly solution to obtain the aeroelastic characteristics inherent in their full-scale counterparts. However, for the scaled results to be representative of the expected ones from the full-scale, a correct scaling that ensures aeroelastic similitude is required [7].

The methodology that enfold an aeroelastic scaling process is often constrained and cut short by the many conflicting requirements [8]. On one hand, restrictions associated with testing facilities limit the design space at early stages and are usually difficult to change or adapt. For instance, the dimension of a wind tunnel test section will bound the overall dimension of the scaled body. On the other hand, scaling requirements are necessary to ensure a proper and valid equivalence between full-scale and scaled models [9]. These scaling parameters, nondimensional by nature, are frequently conflicting and difficult to achieve.

The present work aims to draw novel aeroelastic scaling strategies, that can effectively mitigate the scaling conflicts, expand the design space, and ease the barrier to experimental testing.

C. Additive Manufacturing

One technology that can be leveraged for the purpose of scalability and experimental testing is Additive Manufacturing (AM). AM has seen its application range widen for the past decades, including in the aerospace sector, where it has been used to fabricate wing models and investigate their feasibility and applicability to wind-tunnel tests [10–12], in the design of compact Heat Exchangers [13] or in lightweight aircraft components [14]. This increase in applications is also motivated by the development of new 3D-printing methods throughout the years, expanding the capabilities and applicability of this technology. Nowadays, it is possible to produce highly customised complex structures, at a faster pace, with better quality and precision, and choose from a wider range of materials, from polymers to ceramics and metals [15].

The potential of 3D-printed aeroelastic scaled wing models for flutter wind-tunnel testing stems from the opening of the design space to geometries that were once difficult or impossible to produce, with the possibility of employing multi-material printing to better control the material properties, such as the stiffness [10], and with already successful experimental tests regarding aerodynamics [11, 12]. Nonetheless, there are some drawbacks in 3D printing related to the lack of material directional control during the fabrication process, which can lead to anisotropic mechanical properties [10, 15]. Furthermore, the limitation of available materials can also constrain the design space [15].

D. X-56A Multi-Utility Technology Testbed

The present work takes the X-56A Multi-Utility Technology Testbed (MUTT) [16] aircraft as the body of study for applying the proposed aeroelastic scaling strategies. This flying wing demonstrator was built to be a research platform in the realm of aeroelasticity, and is capable of exhibiting aeroelastic unstable phenomena within its flight envelope, such as body-freedom flutter (BFF) or wing-bending torsion flutter (WBT) [10, 16].

2 AEROELASTIC SCALING STRATEGIES

To create an aeroelastically scaled model, three key properties of the aircraft must be equivalent: structural stiffness distribution, structural mass distribution, and flow similarity. The importance of these properties depends on the particular test being performed. Nevertheless, flutter tests require the similarity of all three properties and are, therefore, the most difficult to reproduce accurately [17].

2.1 Structural sizing and scaled external shape

The simplest method of creating a flutter model is to directly scale down the entire structure of the aircraft to achieve structural similarity and equal external shape. To do so, these criteria between the scaled and original model should be met [18, 19]:

- Same aerodynamic shape;
- Same non-dimensional mode shapes;
- Same Froude number;
- Same set of reduced frequencies;
- Same set of mass ratio;
- Same Mach number is required if compressibility effects are important;
- Same Reynolds number is required if viscous effects are important.

To achieve the correct ratio between all units, the generalised scaling procedure is based on nondimensionalization of the governing equations of motion using the Buckingham π -theorem [20]. References [21–24] resort to this theorem to obtain the scaling laws. Different variables can be considered as elemental, which will then rule the scaling ratios. Depending on the scaling metric, different modal frequencies are obtained, with higher similarity when inertia and structural scaling can be achieved. However, these scaling metrics may give origin to structures that are not realistically feasible [25]. Filippou et al. [17] considered this problem, and constrained the thickness distributions of the scaled model. Since modern aircraft structures are already lightweight and made up of thin components, scaling them down can lead to unrealistic thickness distributions, which pose challenges when manufacturing these components. When all these effects are considered, to regain similarity, the addition of point masses to the computational models is a technique which aims to calibrate the computation models and mainly increases the matching of the modal behaviour and its frequency [4, 7, 26, 27].

2.2 Structural topology optimisation and scaled external shape

A different way of achieving mass and stiffness similarity is to create a brand-new internal structure, not bound to the original one. Applying Topology Optimisation (TO) to the wing allows the definition of a completely new structure, ruled by well-defined constraints, in order to achieve a specific objective, whether it is mass reduction, minimum compliance or, in the case of study, achieving the same mass and stiffness and/or the same static and dynamic structural behaviour as the original model.

Gomes and Palacios [28] used TO for the aeroelastic design of very flexible wings with the goal of minimising wing mass. Large displacements were considered by coupling a Reynolds-averaged Navier–Stokes finite volume solver with a geometrically nonlinear finite element structural solver. For minimum compliance, Wang et al. [29] applied TO to minimise compliance on the inner segment of a three-dimensional Common Research Model wing structure, considering the aeroelastic effect. The optimal wing structure was clear and close to the double-beam configuration in practical engineering, proving the efficiency for the three-dimensional wing structure.

TO applied specifically with aeroelastic scaling in mind was performed by Oliveira et al. [30], which resorted to different TO strategies based on a density approach. Without this metric, the difference between natural frequencies was less than 1%, however, when accounting for manufacturing constraints, such as no allowable intermediate densities and minimum material thickness, the discrepancies increase up to 20%.

2.3 Structural sizing and aerodynamic shape optimisation

Flow similarity might not be possible even if the external geometry is identical. It is challenging to maintain the Reynolds (Re) and Mach (Ma) numbers when scaling the models, and often only possible at the cost of altering some structural properties, such as mass and length ratio, and/or air properties, such as density and temperature [25]. If these two parameters are not the same, flow similarity is not achieved and the scale model aeroelastic response is compromised. In light of this issue, a possible approach to achieve aerodynamic similarity is to allow the wing the freedom to modify its external shape and structure, ensuring that its static and dynamic behaviour remains similar to that of the full scale. Colomer et al. [31] using a multidisciplinary optimisation approach managed to achieve relative differences lower than 1%, with a good agreement for the wingtip displacement, as opposed to 16% using the classical theory.

Further research has been conducted to explore the potential of this strategy. The objective of optimising the aerodynamic properties of airfoils and wings is typically related to reducing drag or increasing the maximum lift coefficient. For aeroelastic optimisation, a fluid-structure interaction is required to assess and maximise the flutter speed. He et al. [32] used a coupled adjoint method which directly deals with the whole aeroelastic system and solves a single adjoint equation, managing to achieve an increase of 10.9% in the flutter velocity.

2.4 Structural topology optimisation and aerodynamic shape optimisation

To overcome some of the structural problems and constraints that can arise from aerodynamic shape optimisation, one could combine this methodology with structural topology optimisation to obtain, in the end, a completely similar scaled model. The combination of both techniques was applied by Hoghoj et al. [33] in order to optimise a wing for cruise conditions by minimising drag. However, the authors stated that in their study, the change in aerodynamic performance due to the wing deflection was neglected since only one-way coupled physics was applied. Additionally, important dynamic effects, such as flutter, were also ignored in this study.

No references were found on coupling both techniques for aeroelastic scaling purposes, and, as seen before, even using each technique separately does not have a strong literature background in this area of study. The challenges for combining these methodologies are immense, as the domain and boundaries for the structural and aerodynamic optimisation are constantly changing throughout the process, and a coupled two-way interaction between both methods is required.

3 METHODOLOGY

The project methodology is built around eight major tasks, presented in Figure 2, which comprise both computational and experimental work. By testing novel aeroelastic scaling strategies on X-56A aircraft, empowered by the synergy of distinct technologies, it is the goal of the project to reduce the barrier to experimental testing, as well as to facilitate aeroelastic analysis in the conceptual phase of aircraft design, possibly expanding its design space. The eight tasks can be grouped into three distinct groups:

1. **Aircraft Model and design constraints:** relative to the first two tasks, it comprises the initial modelling of the X-56A aircraft, aeroelastic analyses and respective validation. An assessment on the various restrictions that can impact the design space and future tasks is performed.
2. **Aeroelastic scaling procedure:** includes tasks three to five, comprising the bulk of the project in terms of work and novelty. The aeroelastic scaling strategies presented in Section 2 are implemented, tested, and validated. The results are compared, leading to the selection of the most promising method.
3. **Experimental testing:** tasks six to eight, referring to the manufacture, instrumentation, and subsequent testing of the X-56A experimental aircraft to validate the chosen aeroelastic scaling strategy. A final assessment is then presented.

This paper concerns the first task of the framework, namely the modelling of the X-56A aircraft geometry, and the need to replicate its mechanical properties and aeroelastic response. Since aeroelastic analyses are to be performed using both low- and high-fidelity software, a link between them is explored. This link allows for the use of low-fidelity software to rapidly evaluate the aeroelastic response over the flight envelope and then migrate to higher-fidelity software around which the scaling strategies are integrated and applied. Due to the high-aspect

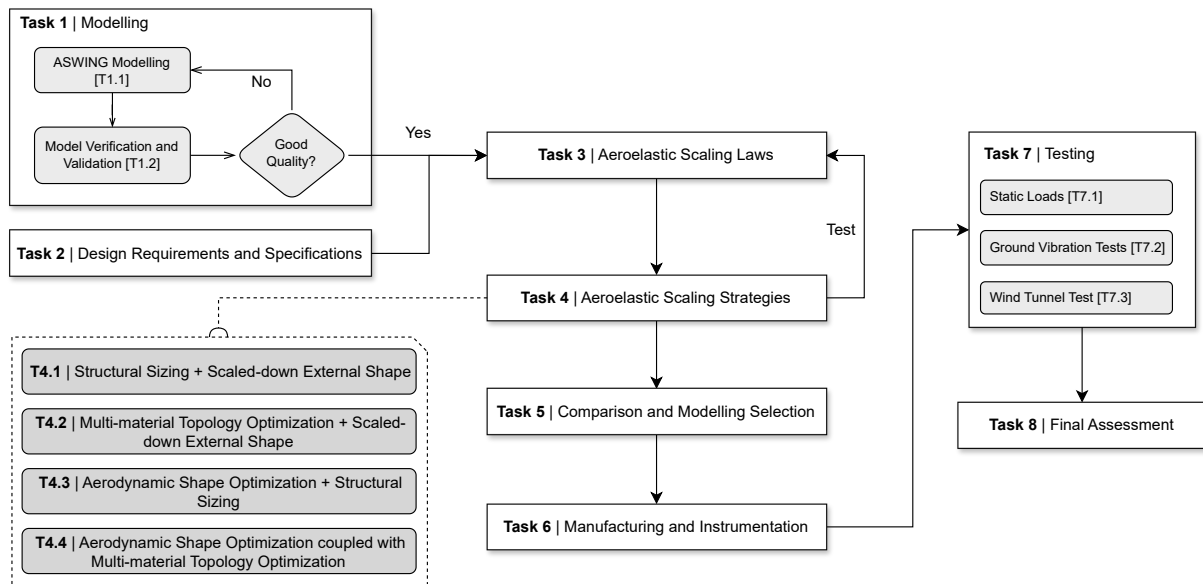


Figure 2: Methodology flowchart comprising the main tasks of this project/work.

ratio of the X-65A, large displacements are present, and thus, simple analyses that resort to linear structural models and to simple aerodynamic models are not enough. Instead, a nonlinear geometrical and structural analysis, large displacements and unsteady aerodynamics must be considered for the results to be in line with experimental data [34, 35].

ASWING, developed by Drela at MIT [36], is a program designed for predicting the static and quasi-static loads, as well as deformations, in aircraft featuring flexible high aspect ratio lifting surfaces and fuselage beams. This low-fidelity framework was validated by comparing 2-D flutter results for a sample wing with Theodorsen [37], obtaining an exact match with its implied flutter methods. Various modules of ASWING were also validated when conducting rigid-structure cases, elasticity with small deflections, divergence, aileron reversal, and flutter speed prediction [38]. References [39, 40] provide experimental data collected in GVT and flight tests and present a good agreement with ASWING results.

MSC NASTRAN is then used as a high-fidelity source to validate the results and carry on with future optimisation and integration work. A proper link between ASWING and MSC NASTRAN, where equivalence in aeroelastic response is met, is of the utmost importance. Although difficult, this equivalence is not unprecedented. Simulations for a flying wing on both ASWING and MSC NASTRAN showed similar results on the flutter speed and frequency, considering different altitudes, weights, and centre of gravity (CG) locations [41].

4 FROM MSC NASTRAN TO ASWING

To obtain a sufficient similarity in the aeroelastic response of an aircraft that has been modelled from two distinct software, MSC NASTRAN and ASWING, it is necessary to understand how both software work, namely the theories and numerical methods each one employs and how the structures can be discretized on the various type of elements. Therefore, to understand the internal structure and overall geometry of the aircraft's model, it is fundamental to accurately devise a proper conversion strategy and acquire valid results.

A. X-56A MSC NASTRAN model

The X-56A aircraft MSC NASTRAN model was made available to the work team and it consists of a detailed finite element model of the entire aircraft, as depicted in Figure 3. The model was generated in MSC NASTRAN and flutter studies were performed using SOL144, which considers the P-K solution method, with the results in accordance with GVT data. The internal structure of the X-56A is composed of 2 main spars and 17 ribs per wing half (Figure 4). Control surfaces are present on the trailing edge of the wing along around 90% of its span. Point masses are added to represent additional components such as engines, fuel and ballast weights [42].

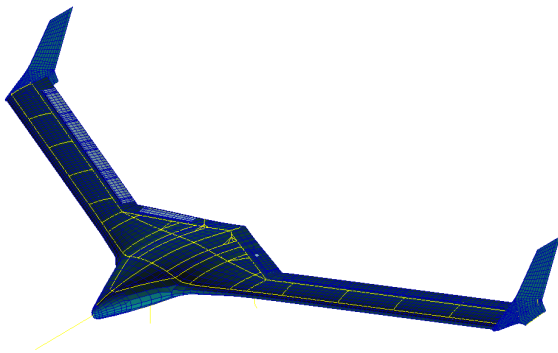


Figure 3: X56-A FEM model.

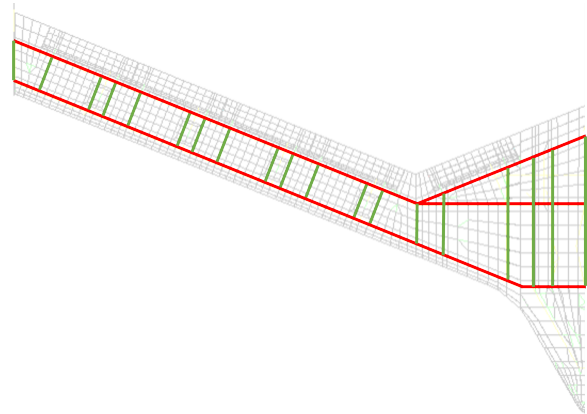


Figure 4: X56-A top view internal structure: ribs displayed in green, spars in red.

B. Geometry modelling

Regarding the modelling of the X-56A aircraft geometry in ASWING, shown in Figure 5 and Figure 6, input data points from the FEM model are being used to define the coordinates of each section reference local system, which are then connected via cubic splines. At each of these sections, ASWING requires some parameters to define the outline of the geometry and the correct computation of the body's static and dynamic responses. One of these parameters is the value of the chord normal to the local system of reference, which is given in terms of relative position to the leading edge. This complicates the geometry definition, possibly leading to saw-like behaviour where more complex shapes or discontinuities exist. Consequently, another approach that manipulates the position of the local reference system is procured. The position of the shear centre is also a relevant input since it constrains the model's response. The current task refers to accurately modelling the swept portion of the main wing, more concretely near the regions of geometric discontinuities.

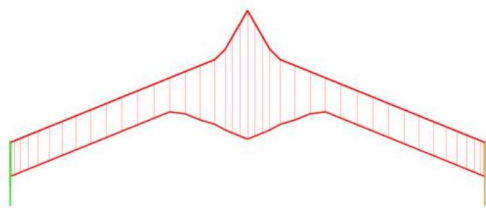


Figure 5: ASWING model top View.



Figure 6: ASWING model side View.

C. Structural model

Figure 7 presents a closer look at the wingbox structure on the second part of the wing (2 spar section). From the BDF file (MSC NASTRAN native file format), it is possible to distinguish different materials, laminates, and properties of the wingbox's various components. All "panels" are modelled as shell elements. Regarding the spars, four bar elements establish the connection between the spar webs and skin and are depicted by red edges in Figure 7. These elements will significantly affect the section's dynamic response. Additionally, along the span, ribs modelled as shell elements are also present between the spars, providing additional torsion stiffness but more importantly, they prevent structural buckling. Moreover, the material properties vary along the span. The laminae materials, laminae orientation and a different stacking sequence can be present, thus providing a variation of the section stiffness properties along the span.

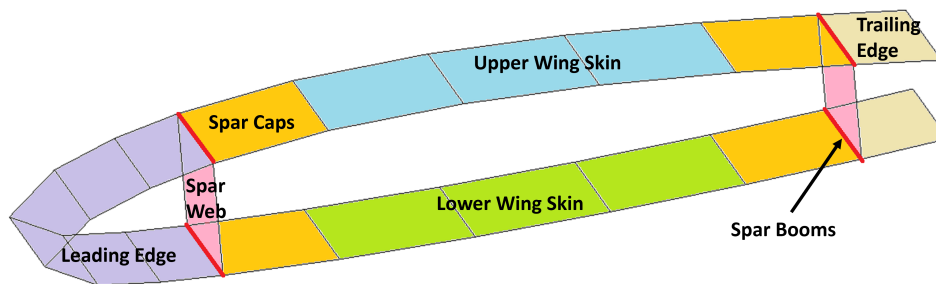


Figure 7: X56-A section cut representing the wingbox.

As ASWING considers a beam-structural model, it is necessary to recreate the inertial, stiffness, and mass properties of the wingbox (see Figure 7) at each section. Given the complex structure of the wingbox, which includes composite materials and boom structures, a stepwise approach is employed. A simple structure is initially created, and the free vibration frequencies are compared between ASWING and SOL103 from MSC NASTRAN. Then, sequentially more complexity is added step-by-step, to be able to recreate the entire wingbox structure at the end.

Since analysing a simple beam on ASWING has been extensively reviewed and tested [36], the first case to test is a simple hollow rectangular cross-section modelled using isotropic shell elements. At this stage, the isotropic materials properties were derived from the real X-56A laminate properties at each region of the wing, at which classical laminate theory (CLT) was applied to extract the equivalent flexural Young and Shear Modulus. The beam length was assumed to be 2.4 m with the cross-section dimensions close to the X-56 ones.

The free model analysis shows a good agreement for both in-plane bending (IPB) and out-of-plane bending (OPB) frequencies with torsion having a big discrepancy (over 25%). Actually, when conducting the modal analysis in MSC NASTRAN, after both bending modes, the next modal modes obtained have a considerable section deformation, which is not possible in the ASWING formulation and may justify the torsion deviation. Additionally, higher-order mode shapes on MSC NASTRAN were buckling modes. To correct this behaviour, ribs were added to both NASTRAN and ASWING models, and the results for all dynamic modes were similar on both software, with deviations under 3% for the first bending modes and under 1% for torsion. In the ASWING model, ribs were accounted by introducing point masses at their span locations.

When considering a multi-cell wingbox, the torsional stiffness and shear centre calculation must be reformulated. Since the cross-section will not deform in the ASWING model, the approach followed by Megson [43] of considering the same rate of twist to all the cells is valid. Additionally, asymmetry on the cross-section must be accounted for, as the shear centre and

centre of gravity must be computed as an input for ASWING.

By adding 1D-bar elements on the spar caps, the local stiffness will increase on that region and will affect the entire wingbox modal behaviour. One should be careful on assuming that the structure is idealised (booms carry most or all bending, wingbox carries torsional loads [43]) just because it has booms. In the case of the X-56A FEM model, the bending stiffness of these bar elements is of the same order of magnitude as the spar web; therefore, all the wingbox structures must be considered for computing the bending stiffness.

To check the ASWING beam formulation at modelling more complex structures, an illustrative 2.4 m semi-span wing with a wingbox structure similar to Fig. 7 was created in MSC Patran, with ribs every 0.3 m. The material properties were the CLT equivalents of the X-56A at a section where the third set of control surfaces are. The same structure was modelled in ASWING. To compute all the cross-section properties, additional features to the initial framework developed by Victorazzo and De Jesus [44] were added, such as calculating the mass moment of inertia. Table 1 displays the obtained results for the first five modes on both MSC NASTARN and ASWING.

Table 1: Sample wingbox beam: MSC NASTRAN vs ASWING

Mode	MSC NASTRAN	ASWING	Difference to MSC NASTRAN
1 OPB	7.902 Hz	7.961 Hz	0.75 %
1 IPB	49.01 Hz	47.88 Hz	2.31 %
2 OPB	51.84 Hz	50.26 Hz	3.05%
1 Torsion	83.68 Hz	83.58 Hz	0.12 %
3 OPB	154.4 Hz	142.8 Hz	7.51 %

The results show a good agreement between both frameworks. One should note the almost perfect match on the torsion mode, which was also achieved for the 2nd torsion mode. The bending modes (both OPB and IPB) present a larger difference, increasing for higher vibration modes which is expected. Nevertheless, since flutter on the X-56A is expected to happen due to the interaction of the first OPB and torsion, or derived from BFF [45], these modes are very well captured on ASWING. Regarding the BFF, one can only compute it on ASWING with aerodynamic data inputs at each cross-section and conduct a modal analysis at various flight speeds [41].

D. Aerodynamic model

To gather the aerodynamic data for the ASWING, for each cross-section along the span, the airfoil points are obtained from the FEM model. Nevertheless, as seen from Figure 7, the mesh is quite coarse, creating a very rough profile to gather any aerodynamic data. Following the work of Palkonien and Reich [10], where the specific cross sections of the airfoils are given in detail, these airfoils are scaled from the real X-56A dimensions and are analysed in XFOIL. Simulations for the airfoils under Reynolds number between 900,000 and 1,500,000 were performed, based on the section chord length and expected flutter speed based on the flight tests [45]. The lift curve slope, drag coefficient and pitch moment coefficient are retrieved with the results hardly varying with Reynolds number or profile analysed. The aerodynamic centre is assumed to be at 25% chord.

5 CONCLUSION

The present work has laid out a foundation for the development of a methodology to explore the feasibility of aeroelastic scaling strategies applied to the X-56A aircraft to enable wind tunnel experimental testing and using topology optimisation methods and additive manufacturing constraints. Four major scaling strategies have been identified: (i) Structural sizing and scaled external shape; (ii) Structural topology optimisation and scaled external shape; (iii) Structural sizing and aerodynamic shape optimisation; and (iv) structural topology optimisation and aerodynamic shape. The manufacture of a scaled model, derived using the proposed methods and manufactured using additive manufacturing techniques, presents the potential to overcome the conflicting scaling parameters, reduce experimental costs, and expand the design feasible space.

The results from the structural modelling show that a good similarity on the modal behaviour of a X-56A wingbox-like structure can be achieved with a lower-order beam modelling using ASWING. However, it is recognised that there are limitations to the proposed methodology, when dealing with complex structural geometries such as control surfaces and associated linkages.

As future work, a full model of the X-56A aircraft in ASWING is currently being performed, to establish a acceptable similarity between the MSC NASTRAN and ASWING modal results.

ACKNOWLEDGEMENTS

The authors acknowledge *Fundação para a Ciência e a Tecnologia (FCT)* for its financial support via the project LAETA Base Funding (DOI: 10.54499/UIDB/50022/2020). Special thanks to Alexander Pankonien and Air Force Research Laboratory (AFRL) for the inputs regarding the methodology definition, possible constraints, and for providing the X-56A aircraft FEM model. The authors are grateful to Professor Mark Drela at MIT for making the ASWING software tool available.

6 REFERENCES

- [1] Palaia, G., Zanetti, D., Salem, K. A., et al. (2021). THEA-CODE: a design tool for the conceptual design of hybrid-electric aircraft with conventional or unconventional airframe configurations. *Mechanics & Industry*, 22, 19. doi:10.1051/meca/2021012.
- [2] Castellani, M., Cooper, J. E., and Lemmens, Y. (2017). Nonlinear Static Aeroelasticity of High-Aspect-Ratio-Wing Aircraft by Finite Element and Multibody Methods. *Journal of Aircraft*, 54(2), 548–560. doi:10.2514/1.C033825.
- [3] Abbott, I. and Von Doenhoff, A. (1959). *Theory of Wing Sections, Including a Summary of Airfoil Data*. Dover Books on Aeronautical Engineering Series. Dover Publications. ISBN 9780486605869.
- [4] Spada, C., Afonso, F., Lau, F., et al. (2017). Nonlinear aeroelastic scaling of high aspect-ratio wings. *Aerospace Science and Technology*, 63, 363–371. doi:10.1016/j.ast.2017.01.010.
- [5] Afonso, F., Lobo do Vale, J., Oliveira, E., et al. (2017). A review on non-linear aeroelasticity of high aspect-ratio wings. *Progress in Aerospace Sciences*, 89. doi:10.1016/j.paerosci.2016.12.004.

- [6] Sundresan, M., Joseph, D. R., Karthick, R., et al. (2012). Review of Aeroelasticity Testing Technology. *Procedia Engineering*, 38, 2297–2311. doi:10.1016/j.proeng.2012.06.276. International Conference on Modelling Optimization and Computing.
- [7] Mas Colomer, Joan, Bartoli, Nathalie, Lefebvre, Thierry, et al. (2022). Aeroelastic scaling of flying demonstrators: mode tracking technique. *Mechanics & Industry*, 23, 2. doi:10.1051/meca/2021051.
- [8] Stanford, B. (2021). Topology Optimization of Low-Speed Aeroelastic Wind Tunnel Models. In *AIAA Scitech 2021 Forum*. (Virtual Event). doi:10.2514/6.2021-1688.
- [9] Wolowicz, C. H., Brown Jr, J., and Gilbert, W. P. (1979). Similitude requirements and scaling relationships as applied to model testing. Tech. rep., NASA.
- [10] Pankonien, A. M. and Reich, G. W. (2018). Multi-Material Printed Wind-Tunnel Flutter Model. *AIAA Journal*, 56(2), 793–807. doi:10.2514/1.J056097.
- [11] Tsushima, N., Saitoh, K., and Nakakita, K. (2023). Structural and aeroelastic characteristics of wing model for transonic flutter wind tunnel test fabricated by additive manufacturing with AlSi10Mg alloys. *Aerospace Science and Technology*, 140, 108476. doi:10.1016/j.ast.2023.108476.
- [12] Moioli, M., Reinbold, C., Sorensen, K., et al. (2019). Investigation of Additively Manufactured Wind Tunnel Models with Integrated Pressure Taps for Vortex Flow Analysis. *Aerospace*, 6(10). doi:10.3390/aerospace6100113.
- [13] Careri, F., Khan, R. H., Todd, C., et al. (2023). Additive manufacturing of heat exchangers in aerospace applications: a review. *Applied Thermal Engineering*, 235, 121387. doi:10.1016/j.applthermaleng.2023.121387.
- [14] Uhlmann, E., Kersting, R., Klein, T. B., et al. (2015). Additive Manufacturing of Titanium Alloy for Aircraft Components. *Procedia CIRP*, 35, 55–60. doi:10.1016/j.procir.2015.08.061. MIC2015, 15th Machining Innovations Conference for Aerospace Industry.
- [15] Ngo, T. D., Kashani, A., Imbalzano, G., et al. (2018). Additive manufacturing (3D printing): A review of materials, methods, applications and challenges. *Composites Part B: Engineering*, 143, 172–196. doi:10.1016/j.compositesb.2018.02.012.
- [16] Ryan, J. J. and Bosworth, J. T. (2014). Current and Future Research in Active Control of Lightweight, Flexible Structures Using the X-56 Aircraft. In *52nd Aerospace Sciences Meeting*. National Harbor, Maryland, USA. doi:10.2514/6.2014-0597.
- [17] Filippou, E., Kilimtzidis, S., Kotzakolios, A., et al. (2024). Towards Structural and Aeroelastic Similarity in Scaled Wing Models: Development of an Aeroelastic Optimization Framework. *Aerospace*, 11(3), 180. doi:10.3390/aerospace11030180.
- [18] Wan, Z. and Cesnik, C. E. S. (2014). Geometrically nonlinear aeroelastic scaling for very flexible aircraft. *AIAA Journal*, 52(10), 2251–2260. doi:10.2514/1.J052855.
- [19] Ricciardi, A. P., Eger, C. A. G., Canfield, R. A., et al. (2014). Nonlinear aeroelastic-scaled-model optimization using equivalent static loads. *Journal of Aircraft*, 51(6), 1842–1851. doi:10.2514/1.C032539.

- [20] Buckingham, E. (1914). On physically similar systems; illustrations of the use of dimensional equations. *Physical review*, 4(4), 345.
- [21] Ouellette, J., Patil, M., and Kapania, R. (2012). Scaling laws for flight control development and testing in the presence of aeroservoelastic interactions. vol. 1. p. 3. doi:10.2514/6.2012-4640.
- [22] Yusuf, S. Y., Hayes, D., Pontillo, A., et al. Aeroelastic Scaling for Flexible High Aspect Ratio Wings. In *AIAA Scitech 2019 Forum*. San Diego, California, USA. doi:10.2514/6.2019-1594.
- [23] Canet, H., Bortolotti, P., and Bottasso, C. (2018). Gravo-aeroelastic scaling of very large wind turbines to wind tunnel size. In *Journal of Physics: Conference Series*, vol. 1037. IOP Publishing, p. 042006.
- [24] Sobron, A. (2018). *On Subscale Flight Testing: Applications in Aircraft Conceptual Design*. Ph.D. thesis. doi:10.3384/lic.diva-152488.
- [25] Afonso, F., Coelho, M., Vale, J., et al. (2020). On the design of aeroelastically scaled models of high aspect-ratio wings. *Aerospace*, 7(11), 166. doi:10.3390/aerospace7110166.
- [26] French, M. and Eastep, F. E. (1996). Aeroelastic model design using parameter identification. *Journal of Aircraft*, 33(1), 198–202. doi:10.2514/3.46922.
- [27] Ricciardi, A. P., Canfield, R. A., Patil, M. J., et al. (2016). Nonlinear aeroelastic scaled-model design. *Journal of Aircraft*, 53(1), 20–32. doi:10.2514/1.C033171.
- [28] Gomes, P. and Palacios, R. (2022). Aerostructural topology optimization using high fidelity modeling. *Structural and Multidisciplinary Optimization*, 65, 137. doi:10.1007/s00158-022-03234-9.
- [29] Wang, X., Zhang, S., Wan, Z., et al. (2022). Aeroelastic Topology Optimization of Wing Structure Based on Moving Boundary Meshfree Method. *Symmetry*, 14(6), 1154. doi:10.3390/sym14061154.
- [30] Oliveira, E., Sohoulı, A., Afonso, F., et al. (2022). Dynamic Scaling of a Wing Structure Model Using Topology Optimization. *Machines*, 10(5), 374. doi:10.3390/machines10050374.
- [31] Colomer, J., Bartoli, N., Lefebvre, T., et al. (2021). An MDO-based methodology for static aeroelastic scaling of wings under non-similar flow. *Structural and Multidisciplinary Optimization*, 63, 1045–1061. doi:10.1007/s00158-020-02804-z.
- [32] He, S., Jonsson, E., Mader, C. A., et al. (2019). Aerodynamic Shape Optimization with Time Spectral Flutter Adjoint. In *AIAA Scitech 2019 Forum*. San Diego, California, USA. doi:10.2514/6.2019-0697.
- [33] Høghøj, L., Conlan-Smith, C., Sigmund, O., et al. (2023). Simultaneous shape and topology optimization of wings. *Structural and Multidisciplinary Optimization*, 66, 116. doi:10.1007/s00158-023-03569-x.
- [34] Su, W., Zhang, J., and Cesnik, C. (2009). Correlations between UM/NAST Nonlinear Aeroelastic Simulations and Experiments of a Cantilever Slender Wing. In *International Forum on Structural Dynamics and Aeroelasticity - IFASD 2009*. Seattle, WA, USA.

- [35] Riso, C. and Cesnik, C. (2021). Correlations Between UM/NAST Nonlinear Aeroelastic Simulations and the Pre-Pazy Wing Experiment. In *AIAA Scitech 2021 Forum*. (Virtual Event). doi:10.2514/6.2021-1712.
- [36] Drela, M. (1999). Integrated simulation model for preliminary aerodynamic, structural, and control-law design of aircraft. In *40th Structures, Structural Dynamics, and Materials Conference and Exhibit*. St. Louis, MO, USA, pp. 1644–1656. doi:10.2514/6.1999-1394.
- [37] Theodorsen, T. (1949). General theory of aerodynamic instability and the mechanism of flutter. Tech. Rep. TR-496, NACA.
- [38] Drela, M. (2015). Aswing 5.99 technical description — steady formulation. *Massachusetts Inst. of Technology, Cambridge, MA*.
- [39] Afonso, F., Lobo do Vale, J., Oliveira, E., et al. (2017). Validation and evaluation of a nonlinear aeroelastic framework using flight test data. In *International Forum on Aeroelasticity and Structural Dynamics - IFASD 2017*. Como, Italy.
- [40] Bras, M., Warwick, S., and Suleman, A. (2022). Aeroelastic evaluation of a flexible high aspect ratio wing uav: Numerical simulation and experimental flight validation. *Aerospace Science and Technology*, 122, 107400. doi:10.1016/j.ast.2022.107400.
- [41] Love, M., Zink, P., Wieselmann, P., et al. (2005). Body Freedom Flutter of High Aspect Ratio Flying Wings. In *46th AIAA/ASME/ASCE/AHS/ASC Structures, Structural Dynamics and Materials Conference*. Austin, Texas, USA. doi:10.2514/6.2005-1947.
- [42] Li, W. W. and Pak, C.-g. (2015). Mass Balancing Optimization Study to Reduce Flutter Speeds of the X-56A Aircraft. *Journal of Aircraft*, 52(4), 1359–1365. doi:10.2514/1.C033044.
- [43] Megson, T. H. G. (2013). *Aircraft Structures for Engineering Students*. The Boulevard, Langford Lane, Kidlington, Oxford, UK: Butterworth-Heinemann, 5th ed.
- [44] Victorazzo, D. S. and De Jesus, A. (2016). A Kollár and Pluzsik anisotropic composite beam theory for arbitrary multicelled cross sections. *Journal of Reinforced Plastics and Composites*, 35(23), 1696–1711. doi:10.1177/0731684416665493.
- [45] Schaefer, J., Suh, P., Boucher, M., et al. (2023). Flying Beyond Flutter with the X-56A Aircraft. Tech. Rep. NASA/TM–20220012337, NASA.

COPYRIGHT STATEMENT

The authors confirm that they, and/or their company or organisation, hold copyright on all of the original material included in this paper. The authors also confirm that they have obtained permission from the copyright holder of any third-party material included in this paper to publish it as part of their paper. The authors confirm that they give permission, or have obtained permission from the copyright holder of this paper, for the publication and public distribution of this paper as part of the IFASD 2024 proceedings or as individual off-prints from the proceedings.